



This is a repository copy of *Full-field analysis of epicardial strain in an in vitro porcine heart platform..*

White Rose Research Online URL for this paper:
<http://eprints.whiterose.ac.uk/140666/>

Version: Published Version

Article:

Ferraiuoli, P., Kappler, B., van Tuijl, S. et al. (4 more authors) (2019) Full-field analysis of epicardial strain in an in vitro porcine heart platform. *Journal of the Mechanical Behavior of Biomedical Materials*, 91. pp. 294-300. ISSN 1751-6161

<https://doi.org/10.1016/j.jmbbm.2018.11.025>

Reuse

This article is distributed under the terms of the Creative Commons Attribution (CC BY) licence. This licence allows you to distribute, remix, tweak, and build upon the work, even commercially, as long as you credit the authors for the original work. More information and the full terms of the licence here:
<https://creativecommons.org/licenses/>

Takedown

If you consider content in White Rose Research Online to be in breach of UK law, please notify us by emailing eprints@whiterose.ac.uk including the URL of the record and the reason for the withdrawal request.



eprints@whiterose.ac.uk
<https://eprints.whiterose.ac.uk/>



Full-field analysis of epicardial strain in an in vitro porcine heart platform

Paolo Ferraiuoli^{a,b,1}, Benjamin Kappler^{c,d,1}, Sjoerd van Tuijl^c, Marco Stijnen^c,
Bas A.J.M. de Mol^{c,d}, John W. Fenner^{a,b}, Andrew J. Narracott^{a,b,*}

^a Mathematical Modelling in Medicine Group, Department of Infection, Immunity and Cardiovascular Disease, University of Sheffield, Sheffield, UK

^b Insigneo Institute for in Silico Medicine, University of Sheffield, Sheffield, UK

^c LifeTec Group, Eindhoven, Netherlands

^d Department of Cardiothoracic Surgery, Academic Medical Center, Amsterdam, Netherlands



ARTICLE INFO

Keywords:

Full-field measurements
Three-dimensional digital image correlation (3D-DIC)
Epicardial strain
In vitro porcine heart
Repeatability
High-resolution

ABSTRACT

The quantitative assessment of cardiac strain is increasingly performed to provide valuable insights on heart function. Currently, the most frequently used technique in the clinic is ultrasound-based speckle tracking echocardiography (STE). However, verification and validation of this modality are still under investigation and further reference measurements are required to support this activity.

The aim of this work was to enable these reference measurements using a dynamic beating heart simulator to ensure reproducible, controlled, and realistic haemodynamic conditions and to validate the reliability of optical-based three-dimensional digital image correlation (3D-DIC) for a dynamic full-field analysis of epicardial strain.

Specifically, performance assessment of 3D-DIC was carried out by evaluating the accuracy and repeatability of the strain measurements across multiple cardiac cycles in a single heart and between five hearts. Moreover, the ability of this optical method to differentiate strain variations when different haemodynamic conditions were imposed in the same heart was examined.

Strain measurements were successfully accomplished in a region of the lateral left ventricle surface. Results were highly repeatable over heartbeats and across hearts (intraclass correlation coefficient = 0.99), whilst strain magnitude was significantly different between hearts, due to change in anatomy and wall thickness. Within an individual heart, strain variations between different haemodynamic scenarios were greater than the estimated error of the measurement technique.

This study demonstrated the feasibility of applying 3D-DIC in a dynamic passive heart simulator. Most importantly, non-contact measurements were obtained at a high spatial resolution (~ 1.5 mm) allowing resolution of local variation of strain on the epicardial surface during ventricular filling. The experimental framework developed in this paper provides detailed measurement of cardiac strains under controlled conditions, as a reference for validation of clinical cardiac strain imaging modalities.

1. Introduction

The quantitative assessment of cardiac strain is increasingly employed in the clinic to evaluate the function of the heart and coronary vessels. Cardiac strain imaging (CSI), may be applied to diagnose myocardial ischemia by detecting reduction in peak systolic strain (Smiseth et al., 2015), to monitor myocardial damage after infarction and to predict patient outcomes during progression of heart failure (Dandel et al., 2009).

Amongst the CSI modalities, ultrasound speckle tracking

echocardiography (STE) is the most frequently used technique because of its relatively simple implementation and wide availability in the clinic (Tee et al., 2013). However, the methodology has fundamental limitations associated with its operating principle as STE typically involves capturing and processing planar cross-sectional views of the heart. This only allows in-plane displacements of cardiac tissue to be detected, thus the out-of-plane motion of the heart (e.g., twisting or torsion) introduces errors that may result in strain artefacts. Moreover, with this technique, the motion of the heart is analysed by tracking tissue features in the image created by acoustic reflections and

* Corresponding author at: Department of Infection, Immunity & Cardiovascular Disease, Faculty of Medicine, Dentistry & Health, University of Sheffield, Medical School, Beech Hill Road, Sheffield, S10 2RX, UK.

E-mail address: a.j.narracott@sheffield.ac.uk (A.J. Narracott).

¹ These authors contributed equally to this publication.

<https://doi.org/10.1016/j.jmbbm.2018.11.025>

Received 11 September 2018; Received in revised form 24 November 2018; Accepted 26 November 2018

Available online 30 November 2018

1751-6161/ © 2018 The Authors. Published by Elsevier Ltd. This is an open access article under the CC BY license (<http://creativecommons.org/licenses/by/4.0/>).

interference patterns, which may not be representative of the actual cardiac tissue displacements. Therefore, verification and validation of this imaging modality are still under investigation (Pettersen et al., 2017).

Although optical surface imaging techniques cannot be employed for non-invasive *in vivo* imaging of human hearts, they can be used to measure strain in *ex vivo* models replicating cardiac function in order to provide data to support the ongoing validation process of STE (Pettersen et al., 2017). In this context, a powerful optical method that performs accurate shape and deformation measurements with a high resolution is three-dimensional digital image correlation (3D-DIC), which consists of combining the DIC method (Sutton et al., 2009) with a stereovision system.

Originating from experimental mechanics, DIC has now been applied in several scientific fields including biomechanics (Palanca et al., 2016). In fact, DIC has been largely adopted to study the mechanical behaviour of biological tissues because it offers non-contact full-field measurements, which are beneficial when studying anisotropic and inhomogeneous materials such as cardiovascular tissues (Bersi et al., 2016; Genovese et al., 2015). DIC usually requires an artificial pattern (speckle pattern) to be applied to the object surface and tracked during deformation (Sutton et al., 2009). More importantly, the speckle pattern quality strongly affects the success and accuracy of DIC analysis (Lecompte et al., 2006). Ensuring appropriate pattern quality can be very challenging in soft tissue because of the moist, reflective surface. To tackle this problem, Lionello et al. (2014) developed an effective procedure to mark porcine ligaments; first staining the sample with a dark dye and later spraying the surface with white speckles. This approach was also used by other researchers to characterise strain in the human tendon (Luyckx et al., 2014) and porcine spine (Palanca et al., 2017). Recently, 3D-DIC has found application within CSI to monitor deformations in a human heart during an open-chest cardiac bypass surgery (Soltani et al., 2018). In this work, the authors showed the potential of DIC to quantify *in vivo* the mechanical response of the RV during the surgical operation. However, the intrinsic complexity of these studies extremely limited the control of the experimental conditions and, especially, the quality of the applied speckle pattern, which, as mentioned previously, plays an important role in DIC accuracy. Therefore, before considering the DIC methodology as a reference for STE validation, a thorough and comprehensive investigation of its metrological performance in this context is required. We have previously reported the errors associated with 3D-DIC measurements in the surface geometry reconstruction of a porcine heart. Errors in the 3D shape measurements, verified using the additive manufacturing (AM) technology, were less than 1% of the field of view of the camera (Ferraiuoli et al., 2017).

The aim of this paper was to explore the feasibility of using 3D-DIC to map full-field strains in an *in vitro* haemodynamically loaded porcine heart platform (Leopaldi et al., 2018). Specifically, performance assessment of the 3D-DIC method was carried out to evaluate:

- The repeatability of 3D-DIC strain measurement over multiple cardiac cycles in the same heart and between heart samples;
- The ability of 3D-DIC to differentiate variation of strain following changes in the loading conditions on the heart.

2. Materials and methods

2.1. Heart harvesting and mounting within the biosimulator platform

Five hearts were obtained from Dutch Landrace pigs. The animals each weighed about 110 kg were slaughtered for human consumption. After the pigs were CO₂ stunned, hung and exsanguinated until death, a parasternal incision was made in the thorax and the inner organs removed en-block. After veterinary investigation of the organs, the lung veins and pulmonary artery were harvested, and the aorta was

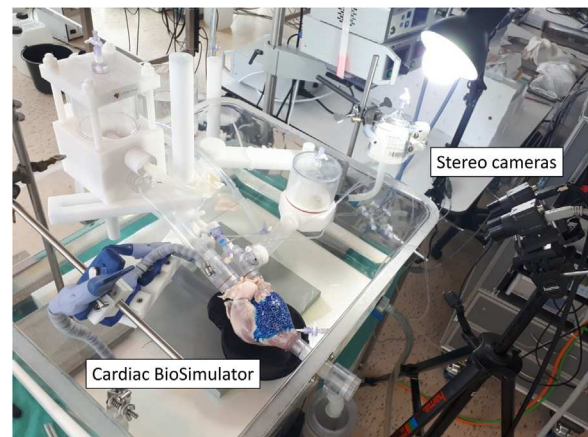


Fig. 1. Picture of the experimental setup including the stereo cameras system and the Cardiac BioSimulator platform (LifeTec, Eindhoven, Netherlands).

transected under the first supra-aortic vessel. The hearts were then isolated and transported to the laboratory. For a more detailed description of the heart preparation, the Cardiac BioSimulator (CBS, LifeTec Group, Eindhoven, NL) see Leopaldi et al. (2018).

Briefly, the aorta and left atrium were cannulated and attached to an external circuit to simulate cardiac cavity circulation, as depicted in Fig. 1. The apex region of the left ventricle was cannulated and connected to a piston pump, which provides pulsatile flow (70 bpm) to the left ventricle by using a pulse duplicator system. The circuit was filled with saline as the working fluid at room temperature. The preload and afterload were adjusted to create a mean preload of 15 mmHg (measured in the left atrium) and an afterload of 80 mmHg (measured in the aorta). The mean cardiac output was set to 3–5 L/min and measured using an ultrasound flow probe (SonoTT™ Clamp-On Transducer, emtec GmbH, Finning, Germany), after the afterload.

2.2. Speckle pattern application and stereo-imaging

The placement of the stereo-imaging system is shown in Fig. 1. To enable DIC measurements, a high contrast stochastic white-on-black speckle pattern was created on the epicardium (Ferraiuoli et al., 2017; Lionello et al., 2014). The cardiac tissue was first soft-brushed with methylene blue (Sigma-Aldrich Company Ltd, Dorset, UK) in order to generate a dark background and improve contrast. An opaque white water-based acrylic paint (Com-Art, Anest Iwata-Medea Inc., Portland, OR, US) was sprayed on the epicardium with an airbrush (Iwata Hi-Line HP-CH, Anest Iwata-Medea Inc., Portland, OR, US) operating with 100 kPa working pressure and a 0.3 mm nozzle diameter at approximately 15 cm spraying distance. Speckle pattern quality was examined through a morphological analysis of the speckles (Lecompte et al., 2006) using custom Matlab code (Matlab R2015b, Mathworks, Natick, MA, US). The speckles had a size of 4 ± 1 pixels, which belonged to the range recommended to avoid aliasing (3–5 pixels (Sutton et al., 2009)).

Camera parameters used in the experiments are described in Table 1. Two synchronised digital CCD cameras (8-bit, Flea2–13S2, Point Grey Research Inc., Vancouver, Canada) equipped with C-mount 25 mm lenses (Comar Optics Ltd, Linton, UK) were arranged in a stereo configuration to capture image pairs during heart deformation (Fig. 1). The cameras were positioned at a distance of approximately 30 cm from the platform. The camera field of view (FOV) was set to image the lateral view of the left ventricle surface as shown in Fig. 2. Upon each test completion, cameras were calibrated to retrieve information on their internal and external parameters using the Matlab Stereo Camera Calibrator application and 25 images of a flat chequerboard with 2 mm internal squares placed at different positions and orientation within the

Table 1
Camera parameters and settings used in the DIC analysis.

Camera parameters	Value
Camera resolution [pixels]	1024 × 768
Image resolution [mm/pixels]	0.05
Magnification	0.08
DIC settings	
Software	Ncorr
Subset size [pixels]	33
Step size [pixels]	9
Interpolation	Biquintic B-spline
Shape function	First-order



Fig. 2. Close-up of the lateral view of the left side of the heart with the applied speckle pattern. The red rectangle identifies the region of interest (ROI) reconstructed in the 3D-DIC measurements.

camera FOV. Mean reprojection errors, a qualitative measure of camera calibration accuracy, were typically 0.3 pixels (0.1 mm) across the experiments.

2.3. Digital image correlation and strain calculation

DIC analysis was performed with Ncorr, an open source 2D subset-based DIC software written in Matlab (Blaber et al., 2015). All DIC settings are given in Table 1. A rectangular region of interest (ROI) was identified in the image of the lateral view of the left ventricle at the lowest ventricular volume (un-deformed state), as shown in Fig. 2. The workflow adopted to perform the stereo-image correlation is illustrated in Fig. 3. Firstly, Ncorr was used to achieve the stereo matching between the corresponding points of the left and right un-deformed images (Fig. 3a). Subsequently, the temporal matching was performed for the left (Fig. 3b) and right deformed images (Fig. 3c), respectively, to track the 2D disparity of the corresponding points during the heart deformation. Finally, using the stereo-camera calibration data and triangulating the corresponding points at each deformed step, the 3D geometry reconstructions of the ROI were retrieved.

Afterwards, by defining a connectivity list between the 3D reconstructed points, surface meshes made of triangular elements at each deformed configuration were generated and used for the strain computation. In particular, full-field surface strains throughout the cardiac cycle were calculated using an approach first proposed by McCulloch et al. (1989) and further investigated by Humphrey (2002) and Genovese et al. (2011). Specifically, components of the deformation gradient tensor \mathbf{F} were computed locally for each flat triangular domain by measuring changes in length of the vectors defined by the triplet of

points on the surface between the reference and current deformed configurations and assuming the deformation to be homogeneous within each element (Humphrey, 2002). Then, the Green-Lagrange surface strain tensor \mathbf{E} was calculated with the equation $\mathbf{E} = (\mathbf{F}^T\mathbf{F} - \mathbf{I})/2$. Finally, from the strain tensor components E_x, E_y, E_{xy} , magnitude and direction of the maximum (E_1) and minimum (E_2) principal strains were obtained by solving the eigenvalue/eigenvector problem of the local strain tensor \mathbf{E}_i ($i = 1, 2, \dots, \text{number of triangular domain}$), respectively.

2.4. Evaluation of strain variation in the unloaded configuration

Whilst the spatial resolution measurement in DIC is influenced by the choice of the subset size, the latter also has an impact on the accuracy and precision. We have previously evaluated the accuracy of the method using a zero strain test, as initially proposed by Smith et al. (1998), which reported errors in strain of 1% (Ferraiuoli et al., 2018). In this study, variation of strain between five successive unloaded configurations was investigated by running a 3D-DIC analysis between images of the heart captured at the beginning of ventricular filling (reference state). The deviation from zero in the strain results was used to assess the variation in strain between each unloaded configuration of the heart, reported as the average (systematic error) and standard deviation (random error) of E_1 and E_2 , respectively, in each heart.

2.5. 3D-DIC repeatability and strain variation assessment

The repeatability of 3D-DIC measurements was quantified between multiple cardiac cycles across the five hearts tested. The intraclass correlation coefficient (ICC) was used to determine the reliability of the strain measurements (Peterson et al., 2017). Based on a two-way random effect model (Koo and Li, 2016), the assessment of 3D-DIC repeatability was performed by comparing the variability of different strain measurements within the same heart to the overall variation across all the measurements and all the five hearts. Specifically, ICC was computed between the average values of E_1 and E_2 , respectively, at the highest ventricular volume states for each individual heart in the different cardiac cycles. With a confidence interval (CI) of 95%, an ICC value lower than 0.5, between 0.5 and 0.75, between 0.75 and 0.9, and greater than 0.9 indicates a poor, moderate, good and excellent reliability, respectively (Koo and Li, 2016).

3. Results

The 3D-DIC analysis was successfully accomplished in all the hearts over a region of the left ventricle surface, however, the reconstructed ROIs were slightly different between hearts because of changes in the anatomical structures and positioning within the cameras FOV.

The strain errors obtained between the five successive reference states of the heart (unloaded configuration) were less than 0.2% in all cases. The median value and range of the average and standard deviation of the surface strain values in the five hearts are reported in Table 2.

The repeatability assessment reported here was performed under the measured haemodynamic parameters reported in Table 3. These were selected for each heart to be within a physiological range. 3D-DIC repeatability assessment was described both quantitatively through the ICC and qualitatively by plotting the average of principal strain surface values over the cardiac cycles, as shown in Fig. 4. The ICC showed an excellent repeatability of 3D-DIC in assessing strains with values of 0.99 for a CI of 95% in both E_1 and E_2 .

As shown in Fig. 4, the frequency of the temporal strain variation in each heart was very similar to the heart rate applied to the pump (70 bpm). Starting from near zero, average strains increased in magnitude as the ventricle expanded and returned to zero at end of the cardiac cycle. The number of mesh triangular elements used in the strain

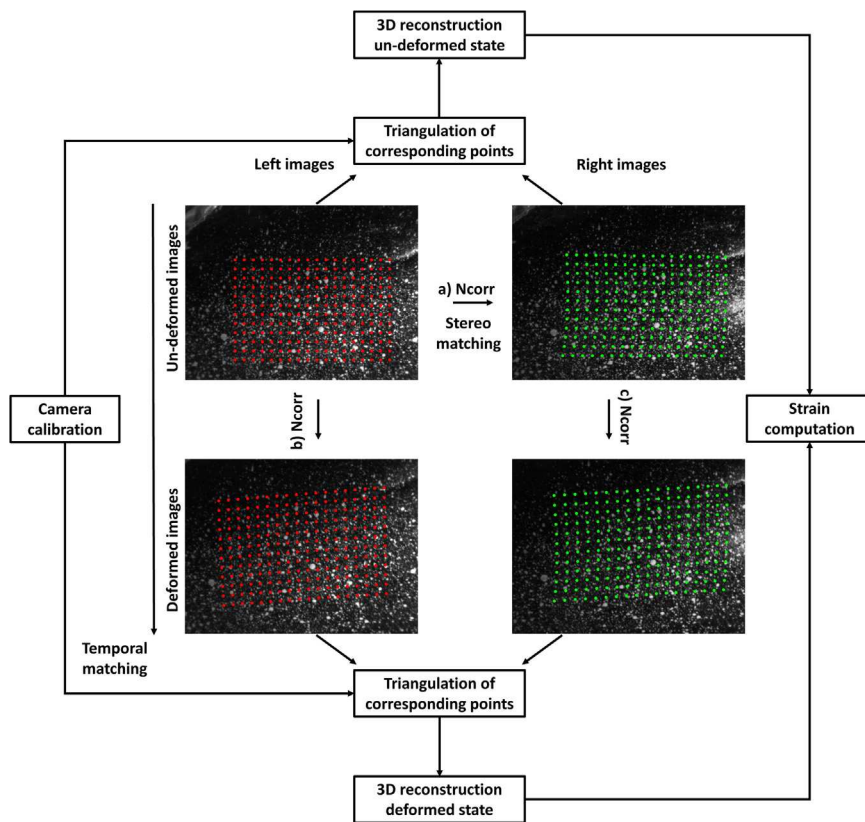


Fig. 3. Schematic representation of the 3D-DIC workflow. a) The corresponding points in the left (red dots) and right (green dots) un-deformed images were found using Ncorr (stereo matching). The displacement of the corresponding points throughout the heart deformation for the left (b) and right (c) deformed images, respectively, was computed with Ncorr. 3D geometry reconstruction in the un-deformed and deformed states was obtained using the camera calibration data and triangulating the corresponding points (For interpretation of the references to color in this figure legend, the reader is referred to the web version of this article).

Table 2

Summary of the systematic (average) and random (standard deviation) zero-strain error over the reconstructed ROIs for the maximum (E_1) and minimum (E_2) principal strain. For each heart, the average and standard deviation of the strain values obtained between three un-deformed images of the heart were calculated. The median and range of the strain values over all five hearts are reported.

	Systematic errors median (min-max) [%]	Random errors median (min-max) [%]
E_1	0.14 (0.08–0.16)	0.12 (0.10–0.15)
E_2	0.09 (0.08 – 0.12)	0.09 (0.09–0.13)

Table 3

Measured haemodynamic and epicardial principal strain values (E_1 and E_2) strain at the end of the highest ventricular volume. For each measurement, the mean and standard deviation for five different heart cycles are given.

	Heart I	Heart II	Heart III	Heart IV	Heart V	
					Normal	Reduced
Haemodynamics						
Minimum aortic pressure [mmHg]	50	55	44	40	45	37
Maximum aortic pressure [mmHg]	109	112	115	109	118	82
Mean aortic pressure [mmHg]	77	82	76	71	79	57
Cardiac output [L/min]	3.4	3.5	4.2	4.2	4.5	1.7
Epicardial strains						
Triangular elements	3780	6100	4730	4510	6120	6120
E_1 [%] (Mean \pm SD)	9.5 \pm 1.5	7.0 \pm 1.0	14.1 \pm 2.5	5.4 \pm 0.9	8.7 \pm 1.1	6.2 \pm 0.1
E_2 [%] (Mean \pm SD)	1.6 \pm 1.0	2.2 \pm 1.2	2.8 \pm 1.4	0.2 \pm 0.6	2.2 \pm 0.7	1.5 \pm 0.0

computation shown in Fig. 4 at the highest ventricular volume state in all the five hearts are reported in Table 3. The number of triangular domains varied between hearts because of the different size of the reconstructed ROI on the epicardial surface. Overall, the area of each triangular facet was approximately 0.15 mm².

The maximum principal strain direction represents the direction of the greatest stretching of the cardiac surface at the highest ventricular

volume and is shown in Fig. 5, along with the minimum principal strain directions, orthogonal to the maximum principal strain directions. The behaviour of the strain distribution throughout the cardiac cycles can be observed in the videos in the Supplementary Materials.

Supplementary material related to this article can be found online at [doi:10.1016/j.jmbbm.2018.11.025](https://doi.org/10.1016/j.jmbbm.2018.11.025).

To demonstrate whether 3D-DIC was able to differentiate haemodynamic changes such as a hypotensive state of the heart (Leopaldi et al., 2015), in one heart (Heart V) the mean aortic pressure was adjusted to 57 mmHg. The strain distribution in the same heart under these different haemodynamic conditions are illustrated in Fig. 6,

showing variation in peak strain between the two states of around 2.5%.

4. Discussion

In this study, a full-field optical technique based on the 3D-DIC method was able to analyse epicardial strains in a dynamic heart model.

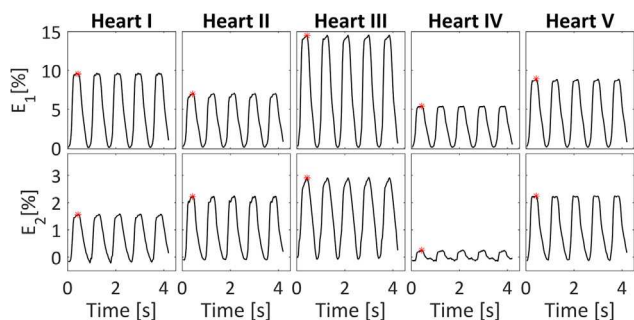


Fig. 4. Average of the maximum (E_1) and minimum (E_2) principal strain distributions over the reconstructed cardiac surface over multiple cardiac cycles in each heart. The asterisks denote the time point at which strain colour map is reported in Fig. 5.

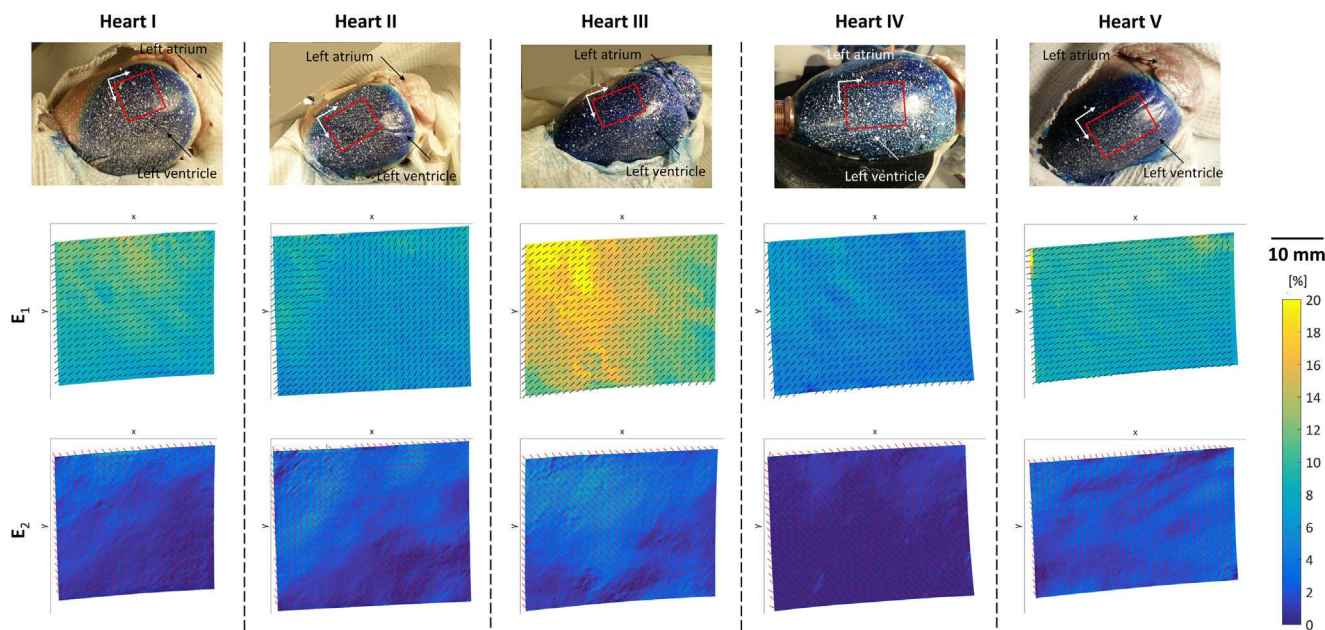


Fig. 5. The five hearts with the approximate location of the ROIs (red rectangular) identified on the left ventricles for the 3D-DIC measurements (upper pane). Strain colour map and directions of maximum (E_1 , middle pane) and minimum (E_2 , lower pane) principal strain on the reconstructed ROIs at the largest ventricular volume state indicated by the asterisk in Fig. 4. The reconstructed surfaces are seen in the xy-plane (For interpretation of the references to color in this figure legend, the reader is referred to the web version of this article).

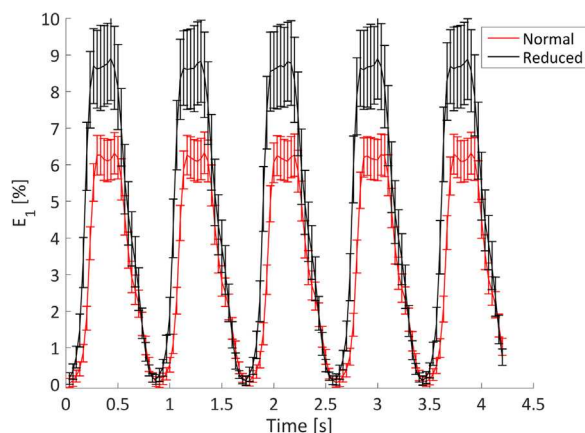


Fig. 6. Comparison between the maximum principal strain (E_1) distributions under two different haemodynamic scenarios imposed on the same heart (Heart V). Mean aortic pressure for Normal and Reduced were 79 and 57 mmHg, respectively. Mean strain value is shown as a solid line, error bars show the standard deviation over the ROI on the cardiac surface at each time point.

Specifically, this work showed the feasibility of performing repeatable and accurate 3D-DIC based strain measurements over multiple cardiac cycles in several hearts. The use of an in vitro cardiac biosimulator platform demonstrated to be valuable for precise, controlled and standardised ventricular deformations obtaining strain measurements directly from soft tissue whilst allowing possible errors in the 3D-DIC measurements to be identified. The DIC analysis was successfully achieved throughout the tests as a result of an adequate speckle pattern created on the cardiac surface. In particular, the coating of the epicardium with methylene blue greatly enhanced the contrast of the white speckles and partially reduced specular reflections, a common problem experienced in the optical imaging of curved objects such as the cardiac surface.

Strain evaluation, performed in the five different hearts, was undertaken while simulating realistic physiological cardiac output and

aortic pressure values (Leopaldi et al., 2018, 2015). Reported strain measures were consistent and highly repeatable over cardiac cycles and hearts (ICC = 0.99). Considerable variation was observed in peak strain magnitude between hearts, as illustrated in Table 3, because of the inherent difference in heart size and ventricular wall thickness. In fact, these effects have been shown to influence the magnitude of epicardial deformations as reported by McCulloch et al. (1989).

In this paper, epicardial strains were expressed in terms of principal strain to remove the dependence on the orientation of the original coordinate system. Moreover, quantification of cardiac mechanical function through a principal strain analysis has been widely carried out because this enables the assessment of the complex behaviour of the myocardium using only normal strain components including their magnitude and directions (Azhari et al., 1993; McCulloch et al., 1989; Waldman et al., 1985; Zhang et al., 2016). The direction of the principal strains was in good agreement over all hearts at the end of ventricular filling, as depicted in Fig. 5. At low ventricular volume, principal strain directions (not reported here for brevity) showed a highly scattered distribution, with ventricular filling the principal directions assumed a consistent pattern. In particular, the first principal strain was typically aligned close to the longitudinal axis of the heart at higher ventricular

volumes with second principal strain in the circumferential direction. Such behaviour has been observed in previous research (McCulloch et al., 1989) where authors demonstrated that during passive ventricular filling maximum extensions become more longitudinal due to muscle fibre orientations. The difference in magnitude between first and second principal strains observed in this work reflects the complex behaviour represented in continuum mechanics models of ventricular filling that assume the passive myocardium to be an anisotropic material affected by the muscle fibre orientation (Gültekin et al., 2016).

Overall, average strain distributions in each heart demonstrated similar time varying form of amplitude and frequency with values at the end of the cardiac cycle very close to zero. These results encourage the use of 3D-DIC to quantify residual tracking errors of STE that have been shown to accumulate over each heart beat (Pettersen et al., 2017). 3D-DIC clearly detected variability in strain distribution between two different haemodynamic scenarios imposed on the same heart, with strain variation larger than the estimated error of the system. Although in this case strain differences reflected changes in the loading condition, the ability to resolve different deformation states of the heart can be used to indicate myocardial dysfunction by measuring the reduction in peak systolic strain (Smiseth et al., 2015). However, in order to accurately detect abnormal strain, a robust and reproducible method is required. Therefore, results reported in this paper promote the use of 3D-DIC to investigate the reliability of clinical imaging modalities such as STE in distinguishing subtle strain variations.

Unlike common schemes employed in DIC to derive strain including filtering (e.g., strain window (Blaber et al., 2015)) and differentiation of the displacement fields (Sutton et al., 2009), in this work, epicardial deformations were evaluated assuming homogeneous strain in each triangular element (Genovese et al., 2011; Humphrey, 2002). Although this approach provided slightly noisier strain distributions and outliers, it allowed a local characterisation of the cardiac surface strain field preserving the original resolution of the DIC measurement (Genovese et al., 2017). Therefore, the subset size selected in the DIC analysis was responsible for the spatial resolution of the measurement (~ 1.5 mm), while the step size defined the number of data points in the 3D reconstructed meshes and the triangles sides (~ 0.5 mm).

Biplane optical techniques have been already examined to study epicardial deformations. Recently, Zhang et al. (2016) presented an optical method to map simultaneously epicardial contraction and membrane potential in beating hearts to study the electromechanical coupling mechanisms. McCulloch et al. (1989) also assessed regional variation of epicardial deformations in the passive heart revealing the anisotropic nature of the cardiac muscle with respect to the muscle fibre directions. However, in these studies, tracking of heart motion was accomplished measuring the displacement of fiducial markers attached to the epicardium that limited the spatial resolution measurement to the number of markers and distance between them (~10 mm). Whereas, in this work, epicardial deformations were retrieved tracking the displacements of the applied speckles which deformed with the underlying tissues to provide a more accurate strain measurement and a higher spatial resolution.

However, some limitations associated with the 3D-DIC method and the experimental platform should be considered in the interpretation of these results. Although an optimisation of the DIC parameters was undertaken to find a compromise between strain uncertainties and a good spatial resolution, 3D-DIC strain results may be affected by other parameters related to both the stereo-optical system (e.g., lens characteristics, image resolution, stereo-angle, and cameras calibration accuracy) and the DIC process (e.g., shape function, correlation criteria and interpolation scheme). Furthermore, synchronisation between camera acquisition and measurements of ventricular volume and pressure change were not available in this study. Thus, the reference image used in the 3D-DIC analysis was determined by identifying the state associated with the lowest ventricular volume of the heart. Moreover, although the CBS platform replicates physiologically

relevant haemodynamic conditions, as the heart is passively distended by an external pump connected to the apex, the ventricular mechanics were not directly comparable with that in a beating heart, which includes three-dimensional dynamic myocardial contraction and ventricular twisting.

5. Conclusions

In vivo techniques currently used to image the heart and perform quantitative assessment of cardiac tissue deformation present some limitations related to the complexity of the scanning protocol (e.g., magnetic resonance imaging, MRI) and assumption of in-plane displacement (e.g., 2D-STE). Full-field optical techniques applied in *in vitro* models of the heart can be used to capture the local behaviour of epicardial strain providing a reference measurement for the validation of these clinical imaging modalities. In this work, an experimental framework combining a highly controlled *in vitro* porcine heart model and the 3D-DIC optical technique has been developed to perform a full-field dynamic analysis of epicardial strain. Highly repeatable and accurate 3D-DIC measurements were obtained over multiple cardiac cycles and different hearts. Most importantly, non-contact measurements were obtained with a higher spatial resolution than other optical techniques allowing resolution of local variations in strain on the epicardial surface. Moreover, the application of DIC enables the collection of highly dense set of data, which may be used to inform mathematical and computational modelling of the heart. Outcomes from this study will support future work to employ the CBS platform as a controlled model of the heart in which to carry out simultaneous measures of cardiac deformations for direct comparison between 3D-DIC and ultrasound strain imaging.

Acknowledgements

This work was funded by the European Commission, Belgium through the H2020 Marie Skłodowska-Curie European VPH-CaSE Training Network (www.vph-case.eu). GA No. 642612.

Ethical approval

All protocols followed by the slaughterhouse and laboratory were consistent with EC regulations 1069/2009 regarding the use of slaughterhouse animal material for diagnosis and research, supervised by the Dutch Government (Dutch Ministry of Agriculture, Nature and Food Quality) and were approved by the associated legal authorities of animal welfare (Food and Consumer Product Safety Authority).

Appendix A. Supporting information

Supplementary data associated with this article can be found in the online version at [doi:10.1016/j.jmbbm.2018.11.025](https://doi.org/10.1016/j.jmbbm.2018.11.025).

References

- Azhari, H., Weiss, J.L., Rogers, W.J., Siu, C., Zerhouni, A., Shapiro, E.P., 1993. Noninvasive quantification of principal strains in normal canine hearts using tagged MRI images in 3-D. *Am. J. Physiol. - Hear. Circ. Physiol.* 264, 205–216.
- Bersi, M.R., Bellini, C., Di Achille, P., Humphrey, J.D., Genovese, K., Avril, S., 2016. Novel methodology for characterizing regional variations in the material properties of Murine Aortas. *J. Biomech. Eng.* 138, 071005. <https://doi.org/10.1115/1.4033674>.
- Blaber, J., Adair, B., Antoniou, A., 2015. Ncorr: Open-Source 2D Digital Image Correlation Matlab Software. *Exp. Mech.* 55, 1105–1122. <https://doi.org/10.1007/s11340-015-0009-1>.
- Dandel, M., Lehmkuhl, H., Knosalla, C., Suramashvili, N., Hetzer, R., 2009. Strain and strain rate imaging by echocardiography – basic concepts and clinical applicability. *Curr. Cardiol. Rev.* 5, 133–148. <https://doi.org/10.2174/157340309788166642>.
- Ferraiuoli, P., Fenner, J.W., Narracott, A.J., 2018. Analysis of speckle pattern quality and uncertainty for cardiac strain measurements using 3D digital image correlation. In: Tavares, J.M.R.S., Natal Jorge, R.M. (Eds.), *VipIMAGE 2017, Lecture Notes in Computational Vision and Biomechanics*. Springer International Publishing, Cham,

- pp. 883–892. https://doi.org/10.1007/978-3-319-68195-5_96.
- Ferraiuoli, P., Taylor, J., Martin, E., Fenner, J., Narracott, A., 2017. The accuracy of 3D optical reconstruction and additive manufacturing processes in reproducing detailed subject-specific anatomy. *J. Imaging* 3, 45. <https://doi.org/10.3390/jimaging3040045>.
- Genovese, K., Lee, Y.U., Humphrey, J.D., 2011. Novel optical system for in vitro quantification of full surface strain fields in small arteries: I. Theory and design. *Comput. Methods Biomech. Biomed. Eng.* 14, 213–225. <https://doi.org/10.1080/10255842.2010.545823>.
- Genovese, K., Leeflang, S., Zadpoor, A.A., 2017. Microscopic full-field three-dimensional strain measurement during the mechanical testing of additively manufactured porous biomaterials. *J. Mech. Behav. Biomed. Mater.* 69, 327–341. <https://doi.org/10.1016/j.jmbbm.2017.01.010>.
- Genovese, K., Montes, A., Martínez, A., Evans, S.L., 2015. Full-surface deformation measurement of anisotropic tissues under indentation. *Med. Eng. Phys.* 37, 484–493. <https://doi.org/10.1016/j.medengphy.2015.03.005>.
- Gültekin, O., Sommer, G., Holzzapfel, G.A., 2016. An orthotropic viscoelastic model for the passive myocardium: continuum basis and numerical treatment. *Comput. Methods Biomech. Biomed. Eng.* 19, 1647–1664. <https://doi.org/10.1080/10255842.2016.1176155>.
- Humphrey, J.D., 2002. *Cardiovascular Solid Mechanics*. Springer, New York, New York, NY. <https://doi.org/10.1007/978-0-387-21576-1>.
- Koo, T.K., Li, M.Y., 2016. A Guideline of selecting and reporting intraclass correlation coefficients for reliability research. *J. Chiropr. Med.* 15, 155–163. <https://doi.org/10.1016/j.jcm.2016.02.012>.
- Lecompte, D., Smits, A., Bossuyt, S., Sol, H., Vantomme, J., Van Hemelrijck, D., Habraken, A.M., 2006. Quality assessment of speckle patterns for digital image correlation. *Opt. Lasers Eng.* 44, 1132–1145. <https://doi.org/10.1016/j.optlaseng.2005.10.004>.
- Leopaldi, A.M., Vismara, R., van Tuijl, S., Redaelli, A., van de Vosse, F.N., Fiore, G.B., Rutten, M.C.M., 2015. A novel passive left heart platform for device testing and research. *Med. Eng. Phys.* 37, 361–366. <https://doi.org/10.1016/j.medengphy.2015.01.013>.
- Leopaldi, A.M., Wrobel, K., Speziali, G., van Tuijl, S., Drasutiene, A., Chitwood, W.R., 2018. The dynamic cardiac biosimulator: a method for training physicians in beating-heart mitral valve repair procedures. *J. Thorac. Cardiovasc. Surg.* 155, 147–155. <https://doi.org/10.1016/j.jtcvs.2017.09.011>.
- Lionello, G., Sirieix, C., Baleani, M., 2014. An effective procedure to create a speckle pattern on biological soft tissue for digital image correlation measurements. *J. Mech. Behav. Biomed. Mater.* 39, 1–8. <https://doi.org/10.1016/j.jmbbm.2014.07.007>.
- Luyckx, T., Verstraete, M., De Roo, K., De Waele, W., Bellemans, J., Victor, J., 2014. Digital image correlation as a tool for three-dimensional strain analysis in human tendon tissue. *J. Exp. Orthop.* 1, 7. <https://doi.org/10.1186/s40634-014-0007-8>.
- McCulloch, A.D., Smail, B.H., Hunter, P.J., 1989. Regional left ventricular epicardial deformation in the passive dog heart. *Circ. Res.* 64, 721–733. <https://doi.org/10.1161/01.RES.64.4.721>.
- Palanca, M., Marco, M., Ruspi, M.L., Cristofolini, L., 2017. Full-field strain distribution in multi-vertebra spine segments: an in vitro application of digital image correlation. *Med. Eng. Phys.* 0, 1–8. <https://doi.org/10.1016/j.medengphy.2017.11.003>.
- Palanca, M., Tozzi, G., Cristofolini, L., 2016. The use of digital image correlation in the biomechanical area: a review. *Int. Biomech.* 3, 1–21. <https://doi.org/10.1080/23335432.2015.1117395>.
- Pettersson, N.J., Fixsen, L.S., Rutten, M.C.M., Pijls, N.H.J., van de Vosse, F.N., Lopata, R.G.P., 2017. Ultrasound functional imaging in an ex vivo beating porcine heart platform. *Phys. Med. Biol.* 62, 9112–9126. <https://doi.org/10.1088/1361-6560/aa9515>.
- Smiseth, O.A., Torp, H., Opdahl, A., Haugaa, K.H., Urheim, S., 2015. Myocardial strain imaging: how useful is it in clinical decision making? *Eur. Heart J.* 37, 1196–1207. <https://doi.org/10.1093/eurheartj/ehv529>.
- Smith, B.W., Li, M., Tong, W., 1998. Error assessment for strain mapping by digital image correlation. *Exp. Tech.* 22, 19–21. <https://doi.org/10.1111/j.1747-1567.1998.tb02332.x>.
- Soltani, A., Lahti, J., Järvelä, K., Curtze, S., Laurikka, J., Hokka, M., Kuokkala, V.-T., 2018. An optical method for the In-vivo characterization of the biomechanical response of the right ventricle. *Sci. Rep.* 8, 6831. <https://doi.org/10.1038/s41598-018-25223-z>.
- Sutton, M.A., Orteu, J.-J., Schreier, H., 2009. *Image Correlation for Shape, Motion and Deformation Measurements*. Springer, US, Boston, MA. <https://doi.org/10.1007/978-0-387-78747-3>.
- Tee, M., Noble, J.A., Bluemke, D.A., 2013. Imaging techniques for cardiac strain and deformation: comparison of echocardiography, cardiac magnetic resonance and cardiac computed tomography. *Exp. Rev. Cardiovasc. Ther.* 11, 221–231. <https://doi.org/10.1586/erc.12.182>.
- Waldman, L.K., Fung, Y.C., Covell, J.W., 1985. Transmural myocardial deformation in the canine left ventricle. Normal in vivo three-dimensional finite strains. *Circ. Res.* 57, 152–163. <https://doi.org/10.1161/01.RES.57.1.152>.
- Zhang, H., Iijima, K., Huang, J., Walcott, G.P., Rogers, J.M., 2016. Optical Mapping of membrane potential and epicardial deformation in beating hearts. *Biophys. J.* 111, 438–451. <https://doi.org/10.1016/j.bpj.2016.03.043>.